PAPER

Motor unit buckling in variable recruitment fluidic artificial muscle bundles: implications and mitigations

IOP Publishing Smart Materials and Structures
Smart Mater. Struct. **31** (2022) 035004 (15pp) https://doi.org/10.1088/1361-665X/ac49d9

Motor unit buckling in variable recruitment fluidic artificial muscle bundles: implications and mitigations

Nicholas Mazzoleni, Jeong Yong Kim and Matthew Bryant

Mechanical and Aerospace Engineering, North Carolina State University, Raleigh, NC 27606, United States of America

E-mail: nwmazzol@ncsu.edu

Received 29 July 2021, revised 7 December 2021
Accepted for publication 10 January 2022
Published 25 January 2022

Abstract

Fluidic artificial muscles (FAMs) are a popular actuation choice due to their compliant nature and high force-to-weight ratio. Variable recruitment is a bio-inspired actuation strategy in which multiple FAMs are combined into motor units that can be pressurized sequentially according to load demand. In a traditional 'fixed-end' variable recruitment FAM bundle, inactive units and activated units that are past free strain will compress and buckle outward, resulting in resistive forces that reduce overall bundle force output, increase spatial envelope, and reduce operational life. This paper investigates the use of inextensible tendons as a mitigation strategy for preventing resistive forces and outward buckling of inactive and submaximally activated motor units in a variable recruitment FAM bundle. A traditional analytical fixed-end variable recruitment FAM bundle model is modified to account for tendons, and the force–strain spaces of the two configurations are compared while keeping the overall bundle length constant. Actuation efficiency for the two configurations is compared for two different cases: one case in which the radii of all FAMs within the bundle are equivalent, and one case in which the bundles are sized to consume the same amount of working fluid volume at maximum contraction. Efficiency benefits can be found for either configuration for different locations within their shared force–strain space, so depending on the loading requirements, one configuration may be more efficient than the other. Additionally, a study is performed to quantify the increase in spatial envelope caused by the outward buckling of inactive or low-pressure motor units. It was found that at full activation of recruitment states 1, 2, and 3, the tendoned configuration has a significantly higher volumetric energy density than the fixed-end configuration, indicating that the tendoned configuration has more actuation potential for a given spatial envelope. Overall, the results show that using a resistive force mitigation strategy such as tendons can completely eliminate resistive forces, increase volumetric energy density, and increase system efficiency for certain loading cases. Thus, there is a compelling case to be made for the use of tendoned FAMs in variable recruitment bundles.

Keywords: bioinspiration, fluidic artificial muslces, variable recruitment, McKibben actuators, motor unit buckling

(Some figures may appear in colour only in the online journal)

1. Introduction

1.1. Fluidic artificial muscles and variable recruitment

Fluidic artificial muscles (FAMs), or McKibben muscles, were first proposed by Joseph McKibben in the 1960s for assisting polio victims [1]. In more recent years, they have emerged as a popular actuation choice due to their compliant nature, ability to interface safely with humans, ease of fabrication, and high force-to-weight ratio. A McKibben muscle consists of an elastomeric bladder surrounded by a braided mesh. When the bladder is filled with pressurized fluid (either pneumatic or hydraulic), the bladder expands radially, and the kinematic constraints imposed by the braided mesh cause it to axially contract. Although some researchers have developed extensile FAMs [2], conventional FAMs are only capable of contracting, as is the case with mammalian muscles. Since they are only capable of contracting, mammalian muscles are arranged in antagonistic pairs to allow for bidirectional motion (e.g. the biceps and the triceps). Likewise, when used in many robotic systems, McKibben muscles are also implemented as antagonistic pairs [3, 4]. However, unlike traditional McKibben muscles, mammalian muscles contain thousands of individual fibers, and these fibers are organized into motor units. Each of these motor units can be activated individually according Henneman's Size Principle, which observes that motor units are activated from smallest to largest depending on the load required [5]. This sequential activation scheme is known as *variable recruitment*. The idea of variable recruitment can be leveraged to improve the performance of hydraulic robotic systems that use McKibben muscles. In conventional hydraulic robotic systems, actuators (hydraulic cylinders or FAMs) are sized for the maximum load required by a given application. However, the actuator may not need to provide this maximum load all the time (or much at all), and in order to provide lower forces, energy is lost due to throttling. However, if smaller actuators are bundled together and arranged into motor units that can be activated individually, then less throttling will be required to operate at lower force regimes, making operation in these regimes much more efficient. Bryant *et al* [6] showed this using an analytic FAM model and an isobaric efficiency calculation. Since this first paper was published, other researchers have experimentally shown that variable recruitment results in efficiency gains in both pneumatic and hydraulic systems [7, 8], developed hybrid switching controllers for variable recruitment artificial muscle bundles [9], and shown that bandwidth and system-level efficiency can also be improved by variable recruitment [10].

1.2. FAM interactions in variable recruitment bundles

The combination of FAMs into a variable recruitment bundle introduces complex interaction effects between the individual FAMs within the bundle. Consider a FAM bundle consisting of three motor units that uses an orderly recruitment scheme. In an orderly recruitment scheme, introduced by Jenkins *et al* [9], as load demand increases, the pressure in motor unit one (MU1) is increased gradually from zero to source pressure, while the other two motor units remain inactive (i.e. vented). When MU1 is active and the other MUs are inactive, the bundle is in the *first recruitment state* (RS1). Once MU1 reaches a specific pressure threshold or other transition criteria [7, 9], MU2 is activated while MU1 is held at source pressure. This is known as the *second recruitment state* (RS2). This pattern continues until maximal activation of all motor units is reached. When implementing an orderly recruitment simulation for a robot arm, Jenkins *et al* [9] used an empirically-corrected FAM model and considered only tensile motor unit contributions to the overall bundle force. However, in reality, during orderly recruitment, inactive or submaximally pressurized FAMs operating at an instantaneous pressure that have a free contraction less than the overall bundle contraction experience compression and generate resistive forces that oppose bundle tension generation. In addition, inactive and low-pressure FAMs have also been shown to exhibit buckling behavior at sufficiently large compressions, an effect that has been repeatedly observed in variable recruitment bundles [6, 7, 12, 13]. A graphical depiction of this buckling behavior is shown in figure 1.

Buckling of inactive and low-pressure motor units during variable recruitment is an issue that has been noted by many researchers [6, 7, 12–15]. Some of the proposed solutions include encasing the bundle in an elastomer matrix to prevent outward deflection [6], pre-straining the FAMs within the bundle to prevent them from entering the buckling regime during contraction [6], and attaching springs to the end of each FAM to prevent buckling [12]. However, while the elastomer matrix prevents outward deflection, it also reduces bundle free strain significantly. In addition, uniform pre-straining of FAMs is difficult in practice, requires an elastic bladder, and most importantly, puts more strain on the bladder, which may decrease its overall lifespan by making it more susceptible to fatigue. Finally, the use of springs reduces overall system stiffness, which may or may not be desirable, and the introduction of springs into the system requires a longer overall system length to provide the same amount of contraction.

1.3. Primary contributions of this paper

In this paper, we investigate a novel resistive force mitigation strategy based on placing inextensible tendons in series with the FAM motor units and compare the resulting bundle actuation performance to the more conventional fixed-end FAM configuration. In section 2 of this paper, we present a mathematical FAM model that captures the effects of motor unit compression and buckling and therefore allows for investigation of motor unit buckling effects and mitigations via tendons. In section 3, we investigate and compare the implications of tendoned and fixed-end motor unit configurations on bundle force and strain production and isotonic efficiency. Finally, in section 4, we discuss how the outward buckling of inactive and low-pressure motor units affects the spatial envelope and volumetric energy density of a variable recruitment bundle and how the proposed configuration mitigates these effects. Section 5 reports the conclusions of the study.

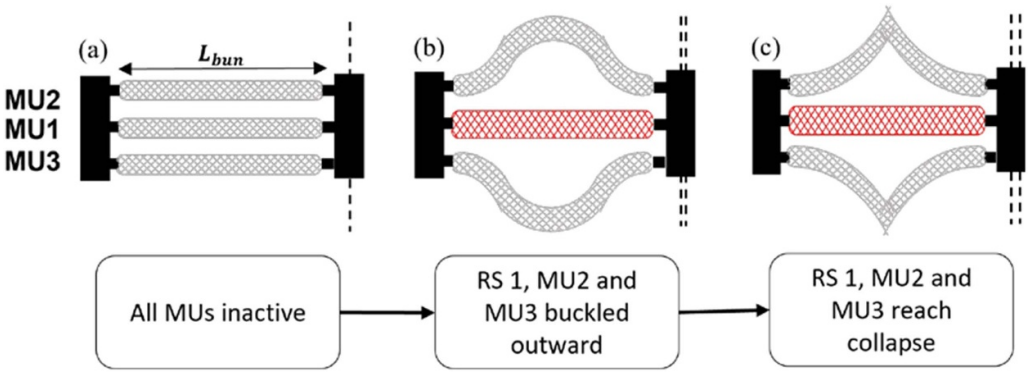

Figure 1. RS1 progression for an orderly recruitment bundle with fixed-end FAMs. The red color of MU1 in (b) and (c) denotes that it is an active FAM, while they gray color of MU2 and MU3 indicates that the FAMs are inactive. As MU1 contracts, MU2 and MU3 buckle outward and eventually collapse, as shown in (b) and (c).

2. System model and problem formulation

2.1. Tendoned and fixed-end bundle configurations

In conventional setups, FAM bundles are typically arranged in a 'fixed-end' configuration. In such an arrangement, one end of the FAM is attached to a fixed endplate, while the other end is attached to an endplate that can translate along with the FAM as it contracts. When MU1 is pressurized in RS1, it starts to contract and the movable endplate begins to translate. Because MU2 and MU3 are rigidly attached to both endplates, they begin to resist motion and eventually buckle and collapse. This progression can be seen in figure 1. Buckling can be detrimental to the performance of a variable recruitment bundle for multiple reasons. For one, when the FAMs in the bundle buckle outward, they generate resistive forces (although the generation of resistive forces is not unique to buckling and occurs any time a FAM is compressed past its free strain). Buckling also increases the spatial envelope of the bundle, which would be problematic in highly spatially constrained applications where tightly packed components are a necessity. Finally, buckling and subsequent collapse of the FAM may shorten the life of the actuator due to stress concentration in the bladder and disturbances to the braided mesh geometry.

As an alternative to existing resistive force mitigation methods, we propose a novel 'tendoned' configuration that uses flexible but inextensible tendons to provide slack for inactive and submaximally activated FAMs, thus preventing them from buckling outward. Figure 2 shows the differences between the fixed-end and the tendoned configurations.

To compare the performance between the tendoned configuration and the fixed-end configuration, the overall length of both systems is kept the same. The overall bundle strain for both configurations is defined as:

$$\varepsilon_{\text{bun}} = \frac{L_{\text{bun}} - L_1}{L_{\text{bun}}} \tag{1}$$

where L_{bun} is the overall system length (also the initial length of MU1) and L_1 is the length of MU1 for a given contraction. The reason why L_1 can be used to describe the bundle strain for both the fixed-end and tendoned configurations is

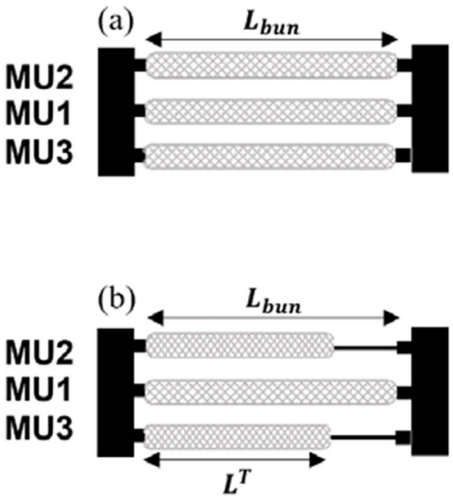

Figure 2. Comparison between fixed-end (a) and tendoned (b) configurations. The two bundle configurations have the same overall length (L_{bun}), while MU2 and MU3 are shorter for the tendoned configuration (both have a length of L^{T}).

because the first motor unit in the tendoned configuration is the same length as the first motor unit in the fixed-end configuration. This is because in an orderly recruitment scheme, MU1 will never be in compression, precluding the need to prevent resistive forces. The remaining motor units contain FAMs with shorter lengths due to the presence of the tendons and the bundle length constraint. To properly size tendons, it is important to understand what objective we wish to accomplish through the use of the tendons. For example, if we want to prevent resistive force and compression throughout the full range of bundle contraction, we need to size the tendons such that they are greater or equal to the maximum contraction of the first motor unit, i.e.

$$L^{\text{T}} \geq L_{\text{bun}}\varepsilon_{\text{bun,free}} \tag{2}$$

where L^{T} is the length of a tendoned FAM and $\varepsilon_{\text{bun,free}}$ is the overall bundle free strain at source pressure. In some applications, FAMs are never operated near free strain because larger forces are required. In such cases the tendon length (and

associated FAM length) for subsequent MUs could be adjusted. These sizing considerations are significant because when both bundle configurations are required to have the same overall system length, a MU with a tendon attached will have less overall contraction than its fixed-end counterpart because it will have a shorter length FAM. The free strain of a tendoned configuration MU can be mapped to the free strain of a fixed-end MU (also referred to as bundle free strain) by using the following equation:

$$\varepsilon^{\mathrm{T}}_{\mathrm{free},N} = \varepsilon_{\mathrm{bun,free}} \frac{L^{\mathrm{T}}_N}{L_{\mathrm{bun}}} \tag{3}$$

where $\varepsilon_{\mathrm{bun,free}}$ is the bundle fixed-end free strain and L^{T}_N is the initial FAM length for the Nth tendoned MU. As a result of this relationship, bundles in the tendoned configuration will have a smaller operating space than bundles in the fixed-end configuration. This will be examined in detail in section 3 of this paper for a bundle consisting of three MUs.

2.2. Modeling FAM tension and compression

Before we can understand the differences between the fixed-end (which will experience resistive forces) and tendoned (which will not experience resistive forces) bundle design configurations, the following requirements for the model of an individual FAM must be met:

- The model must account for the kinematic force of the FAM due to the braided mesh and applied pressure.
- The model must account for the pressure-dependent free strain of the FAM due to the elasticity of the bladder.
- The model must be able to accurately predict resistive forces exerted by post-buckled or post-collapse FAMs within the variable recruitment bundle.

Several models have been used previously in the variable recruitment literature. The ideal FAM model, as presented by Tondu [1], is purely kinematic and does not account for any elasticity effects in the bladder, nor does it consider resistive forces due to FAM compression. Several models account for the pressure-dependent free strain behavior by using a first-principles approach that considers the hyperelasticity of the bladder material [16–19], while other models use semi-empirical correction factors to tune the ideal model according to the actual free strain, rather than the predicted free strain [20–22]. The semi-empirical approach can provide a more accurate model up until free strain, but it requires experimental data and is not valid in the resistive force regime that occurs past free strain. The model recently developed by Kim *et al* [15] accounts for the kinematic force, pressure-dependent free strain, and is valid past free strain, accurately predicting the post-buckled and post-collapse behavior of low-pressure and inactive FAMs. As a result, this model will be used to analyze the effect of resistive forces within a variable recruitment bundle and investigate resistive force mitigation strategies. This model is piecewise in three parts, with each part corresponding to a different part of the force–strain curve: (a) before free strain, (b) after free strain (also called post-buckling), and (c) post-collapse. The first equation in this piecewise model is the equation used to characterize the force generated by a FAM before free strain. To do this, the Klute and Hannaford model [16] is used, which is derived based on the following force balance:

$$F_{\mathrm{total}} = F_{\mathrm{mesh}} + F_{\mathrm{bladder}} = P\frac{dV}{dL} - V_{\mathrm{bladder}}\frac{dW}{dL} \tag{4}$$

where F_{mesh} is the kinematic force generated by the FAM braid, F_{bladder} is the elastic force exerted by the bladder, V_{bladder} is the bladder volume, P is the applied pressure, V is fluid volume, L is FAM length, and W is a Mooney–Rivlin strain energy function. This model predicts pressure-dependent free strain behavior in FAMs because it accounts for the bladder elastic forces and remains valid past free strain.

Once a FAM reaches free strain, it is governed by the post-buckling equation in the piecewise model:

$$F_{\mathrm{total}} = F_{\mathrm{mesh}} + F_{\mathrm{bladder}}\left(\varepsilon_{\mathrm{free}}\right) + F_{\mathrm{pb}} \tag{5}$$

where F_{mesh} is the axisymmetric mesh force generated by the collapsing braid, F_{pb} is the post-buckling force generated by the bladder after free strain, and $F_{\mathrm{bladder}}\left(\varepsilon_{\mathrm{free}}\right)$ is the elastic force generated by the bladder at free strain. Eventually, at high enough strains and/or low enough pressures, the FAM bladder will collapse. This collapse point is determined by the internal collapse moment of the bladder itself. The equation that governs the post-collapse behavior of the FAM is given by the following:

$$F_{\mathrm{total}} = F_{\mathrm{c}} + \left(F_{\mathrm{pb}} - F_{\mathrm{c}}\right) e^{\ \beta(\varepsilon\ \ \varepsilon_{\mathrm{c}})} \tag{6}$$

where F_{c} is the bladder force exerted at collapse (derived using variational methods), ε_{c} is the strain at collapse, and β is a rate transition constant (that can be tuned manually or with parameter optimization) that governs how the bladder force evolves with strain in the post-collapse region. A representative plot of the different regions of the Kim model is shown in figure 3.

While quantitative agreement of this model with experiments can be improved with empirical tuning, we will use the basic analytic formulation described above to facilitate studies over a broad range of parameters. This above model is suitable for this study because it accounts for resistive forces generated by FAMs in compression in the fixed-end configuration, including pre-buckled, post-buckling, and post-collapse behaviors as well as typical tensile FAM operation. For application to the tendoned configuration, the same model is employed but with zero force past free strain as the tendons are assumed to be flexible (yet axially inextensible) such that they exert negligible force in compression. Figure 4 qualitatively illustrates how the tendons accomplish their intended purpose.

When MU1 contracts, the tendons attached to MU2 and MU3 go slack, preventing these motor units from going into compression and generating resistive forces. When an additional MU is activated, it must overcome the slack in its tendon before it can contribute any force to the bundle output.

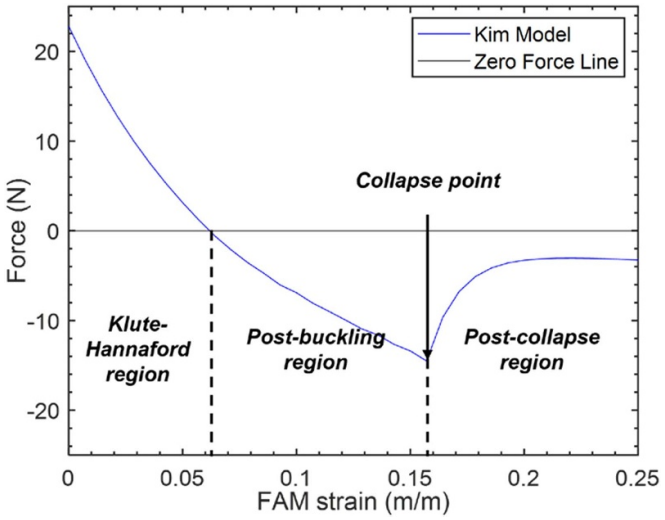

Figure 3. Breakdown of different regions of the piecewise Kim model for a fixed-end FAM with initial outer radius of 6.35 mm, initial braid angle of 33 degrees, initial length of 127 mm, and wall thickness ratio of 0.25. The source pressure is 34.47 kPa. Before free strain, the model is identical to the Klute-Hannaford model. After free strain, the model enters the post-buckling region until it reaches its collapse point, at which the magnitude of resistive force is a maximum. After this point, it enters the post-collapse region, in which the magnitude of resistive force decreases and eventually reaches steady-state.

The pressure required to overcome this slack will be referred to as the 'de-slacking' pressure. A plot of the de-slacking pressure vs. strain for an individual FAM from both the analytical model (specifically equation (4), which describes the tensile part of the piecewise FAM model) and experimental measurements is shown in figure 5.

The experimental data for the MU was obtained using a custom linear hydraulic testing platform which prescribes and records FAM contraction via a double acting hydraulic cylinder (TRD Manufacturing MH series, 2.5 inch bore, 1 inch rod diameter) and LVDT position sensor (RDP Group ACT series) while measuring FAM force with an inline load cell (Transducer Techniques SSM-1 K). The implementation and operation of the apparatus are described in detail by Chipka *et al* and Kim *et al* [15]. As can be seen in the figure, the analytical model underpredicts the de-slacking pressure when compared to the experimental data. However, the results contain the same trends and match closely enough to justify the use of the analytical model to generate bundle force–strain characteristics for the subsequent efficiency and volumetric envelope analyses in this paper.

3. Comparison of tendoned and fixed-end bundle actuation and efficiency

3.1. Case 1: fixed-end and tendoned bundle comparison with equal FAM radii (ER case)

We will now compare the force–strain spaces for two three-MU bundles consisting of one equally sized FAM in each MU for both the fixed-end and tendoned configurations. This case will be referred to as the 'equal radius' (ER) case. For the fixed-end configuration, the total bundle force is taken as the summation of forces from all FAMs, including the negative (resistive) forces predicted by the model for FAMs compressed past their free strain at a given recruitment state and pressure application. For the tendoned configuration, since the tendons are assumed to contribute zero stiffness in compression, only tensile force contributions of the FAMs (as modeled by equation (4)) are included in the total bundle force. The force–strain comparison of the two configurations is shown in figure 6.

From the figure, we observe that for the tendoned configuration, MU2 and MU3 stop contributing force to the bundle at strains less than the overall system free strain. This is because after a certain point, which is determined by the tendon length and free strain of MU1, the only force generated by the tendoned configuration bundle is from MU1 since the tendoned FAMs are shorter and provide less contraction. In figure 6, for each line of constant pressure in RS2 and RS3, the point at which the tendon FAMs stop contributing to overall force corresponds with the de-slacking pressure and associated strain values plotted in figure 5. A shorter tendon length than the one in this study would introduce resistive forces and buckling behavior into the tendoned configuration, but would shift the point at which MU2 and MU3 stop contributing force to higher strain values. Since all three MUs in the fixed-end configuration are the same length, this does not occur, allowing the fixed-end configuration to have a larger potential operating space than the tendoned configuration. The implications of this will be discussed in further detail later in this paper.

In the fixed-end configuration, overlap between recruitment states as a result of resistive forces can be observed. This overlap has been shown both experimentally [14] and in the analytical model developed by Kim *et al* [15]. However, this overlap does not exist in the tendoned configuration plots. Rather, figure 6(b) shows that for the tendoned configuration, when the force value of a particular recruitment state during submaximal activation intersects with the force value of the previous recruitment state at full activation, instead of overlapping, the force values in the two recruitment states simply converge for the remainder of the force–strain space. The motor unit pressure at which this convergence occurs for a given strain and recruitment state corresponds to the de-slacking pressure of the particular FAM in that motor unit.

We next compare the fixed-end and tendoned configurations using isotonic actuation efficiency as a performance metric to explore what tradeoffs occur between the two and in what situations it is beneficial to use one configuration over the other. Following the formulation of Meller *et al* [7], the variable recruitment bundle is used to actuate a prescribed constant load to a desired final strain, as shown in figure 7. The work output required to actuate this load is given by:

$$W_{\text{isotonic}} = F_{\text{load}} L_{\text{bun}} \varepsilon_{\text{bun,des}} \tag{7}$$

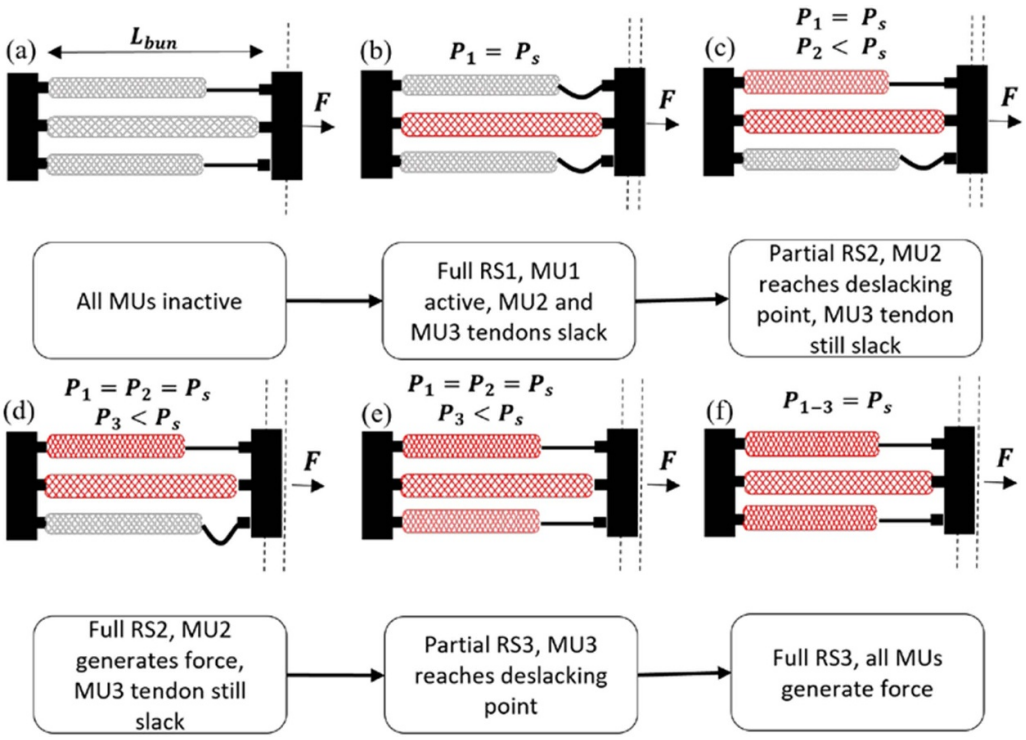

Figure 4. Illustration of variable recruitment scheme with the tendoned configuration. All FAMs are inactive in (a). Red FAMs are active, while gray FAMs are inactive. A clear contrast between the tendoned and previously shown fixed-end configuration can be seen here, as in the tendoned configuration, the tendons attached to the inactive FAMs become slack and therefore prevent the FAMs from buckling outward or generating resistive forces. This slacking effect can be seen in (b)–(d). All three FAMs are fully active in (f).

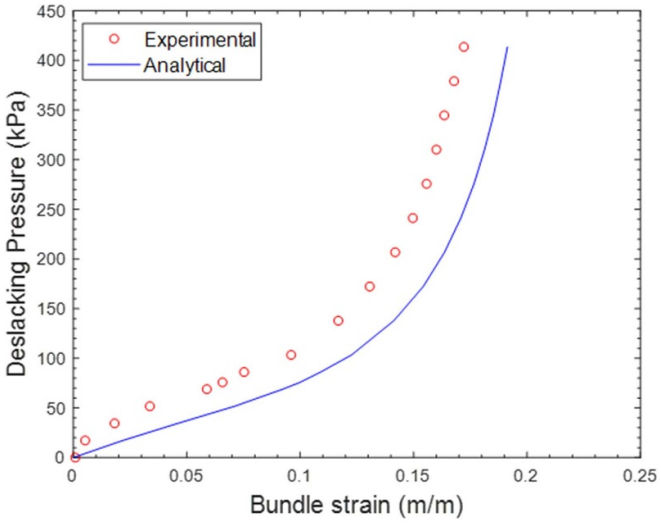

Figure 5. Analytical (from equation (4)) and experimental de-slacking pressure vs. strain for the tendoned configuration. The FAM has an initial outer radius of 6.35 mm, an initial inner radius of 4.76 mm, an initial braid angle of 33 degrees, and a length of 94.2 mm. The inverse of this plot (i.e. free strain as a function of pressure) would correspond to the pressure-dependent free strain curve for the individual FAM. The analytical model underpredicts tendon de-slacking pressure (i.e. overpredicts free strain), but maintains the same trends and characteristics as the experimental results.

where F_{load} is the required load and $\varepsilon_{\text{bun,des}}$ is the desired system strain. The fluid energy input to the bundle is defined as:

$$E_{in} = P_s \Delta V_{RS,\,max} \tag{8}$$

where P_s is the source pressure (the sum of the activation pressure and the pressure drop due to throttling in any associated control valving) and $\Delta V_{\text{RS, max}}$ is the volume change required to reach the necessary recruitment state to achieve the required load at the desired strain. The isotonic efficiency is then given by:

$$\eta = \frac{W_{\text{isotonic}}}{E_{\text{in}}}. \tag{9}$$

We first compare the fixed-end configuration and the tendoned configuration with FAMs of ER and full tendon length (i.e. with tendons sized such that no MU will experience compression for the full strain range of bundle). Figure 8 shows isotonic efficiency surface plots over the force–strain spaces for both the fixed-end and the tendoned bundle configurations

Both configurations would perform favorably over a single equivalent motor unit (as has been shown in [10, 20]), and the tendoned configuration maintains similar isotonic efficiency to the fixed-end configuration in their shared operating spaces. To better visualize the efficiency differences, we can calculate

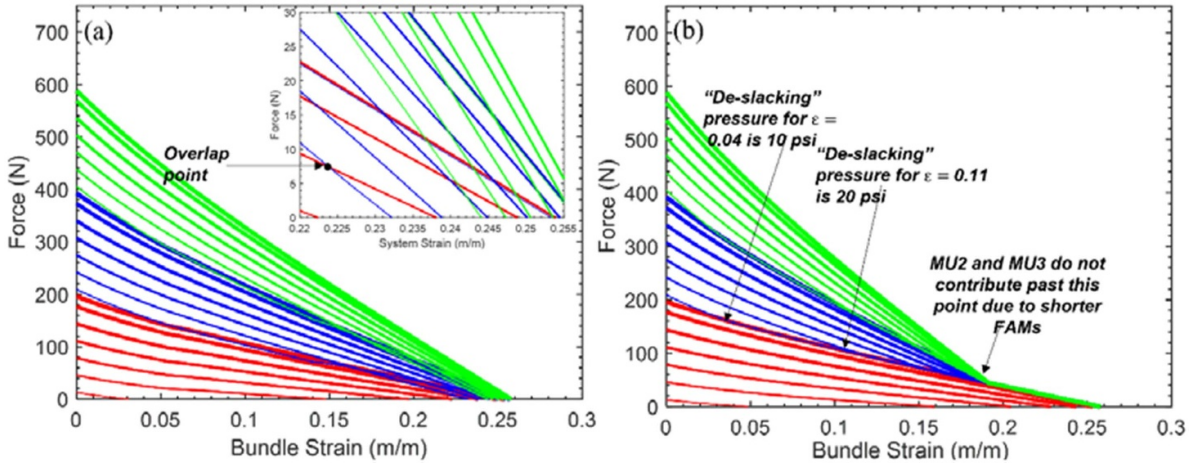

Figure 6. Model-predicted force–strain plots for the fixed-end (a) and tendoned (b) configuration in 68.95 kPa (10 psi) increments. Each MU contains a single FAM with an initial outer radius of 6.35 mm, an initial inner radius of 4.76 mm, an initial braid angle of 33 degrees, and an overall bundle length of 127 mm. For the tendoned configuration, the FAMs in MU2 and MU3 have a length of 94.2 mm to account for the presence of the tendons and to preserve overall system length in both configurations. Varying line thickness is used to indicate pressure in each motor unit, and color is used to represent different recruitment states (red is RS1, blue is RS2, and green is RS3). Recruitment state overlap can be observed in the fixed-end force–strain space. In the inset figure, some (but not all) of the overlap points have been denoted with a black dot to demonstrate this effect. In the tendoned force–strain space, the de-slacking phenomenon can clearly be observed. Due to the equal system length constraint imposed on each bundle, the system free strain of the FAMs in MU2 and MU3 is less than that of the fixed-end configuration, since these are tendoned FAMs and must be shorter. As result, these MUs do not contribute force past a certain point, as reflected in the figure.

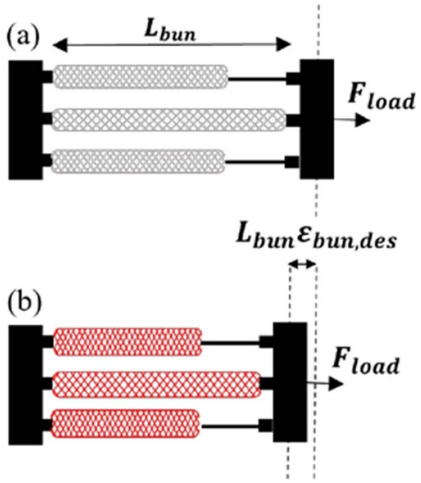

Figure 7. Graphical depiction of loading scenario for calculating isotonic work output and efficiency. The FAMs in (a) are inactive, and the FAMs in (b) are active.

the efficiency difference between the two configurations, given by:

$$\Delta\eta = \eta^{\mathrm{T}} - \eta^{\mathrm{FE}} \tag{10}$$

where η^{T} is the isotonic efficiency of the tendoned configuration and η^{FE} is the isotonic efficiency of the fixed-end configuration.

The surface plot of this efficiency difference is shown in figure 9.

While the fixed-end configuration can provide actuation over a wider space than its tendoned counterpart, we focus on the shared force–strain space between the two configurations. In this shared space, the tendoned configuration experiences modest efficiency benefits over the fixed-end configuration for large parts of the space. However, there exist two important discontinuities within this shared space that occur at the boundaries of RS1 and RS2 and RS2 and RS3, respectively. Between RS1 and RS2, there is a small sliver for which the efficiency benefits of the tendoned configuration are particularly pronounced; this is because in the fixed-end configuration, the presence of resistive forces triggers a recruitment state transition at a lower strain value, resulting in decreased efficiency. Meanwhile, between RS2 and RS3, the fixed-end configuration experiences higher efficiencies than the tendoned configuration because of the reduced length of MU2 and MU3 in the tendoned configuration, making the transition from RS2 to RS3 happen sooner than it does in the fixed-end configuration, resulting in decreased efficiency. The average efficiency of the fixed-end configuration within the entire shared force–strain space is 0.383, while the average efficiency of the tendoned configuration over this space is 0.353. However, as the efficiency difference plots show, this discrepancy is largely due to one particular region of the force–strain space. For the remainder of the force–strain space, the tendoned configuration performs comparably, if not better, than the tendoned configuration. Selection of which configuration to use for a particular application, based on this criterion, would be highly situational and dependent on the region of the force–strain space for which the predominant operation would take place. For example, if it is known *a priori* that the desired motion or loading will remain within the region of the force–strain space for which the tendoned configuration is favorable, then it would make sense, purely from an efficiency standpoint,

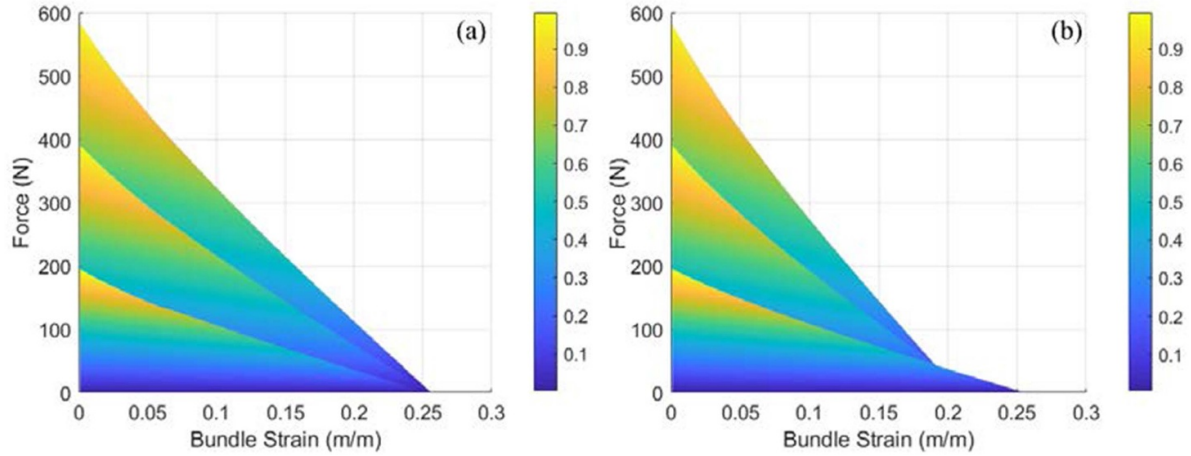

Figure 8. Isotonic efficiency surface over the entire force–strain space for fixed-end (a) and tendoned (b) configurations. The colorbar denotes the magnitude of isotonic efficiency. Both bundles contain three MUs, each containing one FAM with an outer radius of 6.35 mm and initial braid angle of 33 degrees. In the fixed-end bundle, each FAM has a length of 127 mm, while in the tendoned configuration, the FAM in MU1 has a length of 127 mm while the FAMs in MU2 and MU3 both have a length of 94.2 mm to account for the inclusion of tendons.

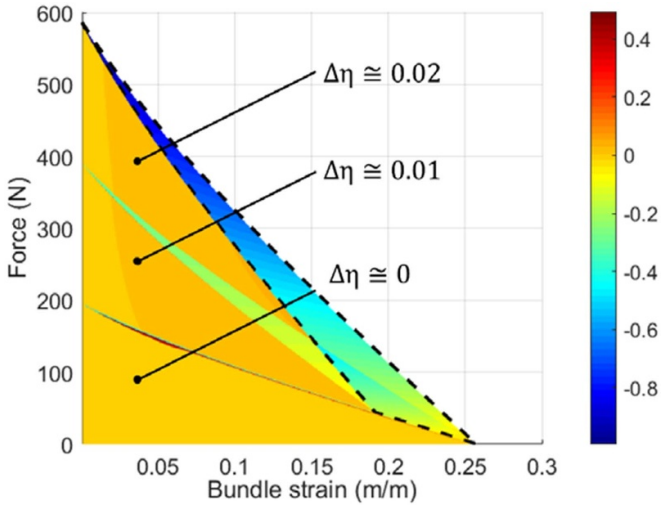

Figure 9. Surface plot of the efficiency difference between the tendoned and fixed-end configurations for the ER case. The FAMs in each MU have the same parameters as the FAMs from figure 8. The area enclosed by the dotted lines represents the part of the force–strain space where the fixed-end configuration can provide actuation but the tendoned configuration cannot due to the reduction in overall contraction in the tendoned FAMs (resulting from their shorter lengths).

to select the tendoned configuration. On the contrary, if the opposite were true, then the fixed-end configuration would be the logical choice if efficiency is the most important metric.

3.2. Case 2: fixed-end and tendoned bundles sized for equal volume consumption (EVC case)

The presence of tendons, combined with the imposed bundle length constraint, result in shorter FAMs in the tendoned configuration (with the exception of MU1) than in the fixed-end configuration. As a result, if the tendoned and fixed-end FAM radii are equal, the fixed-end bundle will consume more working fluid volume than the tendoned FAM bundle. We can, however, size the tendoned FAMs to guarantee that the volume consumption of both configurations is equivalent at maximum strain. To do this, we equate the volume change of the fixed-end and tendon configurations, and use the initial wall thickness ratio, definition of FAM contraction function, and the assumption that the bladder material is incompressible (i.e. volume is conserved throughout contraction) to find the parameters of tendoned FAMs that would result in equal volume consumed for both configurations. The force–strain plot comparison between the fixed-end and the tendoned configurations for equal volume consumption (referred to as the EVC case) is shown in figure 10.

From the comparison plots, it can be observed that for the EVC case, the blocked forces in RS2 and RS3 are larger for the tendoned case due to the larger radii in MU2 and MU3. Figure 11 shows the efficiency difference between the fixed-end and tendoned configurations for the EVC case.

The EVC efficiency difference plots differ from the ER efficiency difference plots in several ways. For one, while both plots contain a region in which the fixed-end configuration can provide actuation where the tendoned configuration cannot, in the EVC plot, there is a region in which the tendoned configuration can meet higher force demands than the fixed-end configuration while operating at the same strain. This is due to the larger FAMs in MU2 and MU3 for the EVC case. Additionally, contrary to the ER case, where the tendoned configuration was favorable to the fixed-end configuration for the majority of the space, in the EVC case, the opposite is true. The fixed-end configuration is favorable over much of the space, with the tendoned configuration having a local region of favorability occurring at the boundary between recruitment RS2 and RS3. This is because of the additional force capabilities of the larger MU2 FAM, allowing the tendoned configuration to remain in

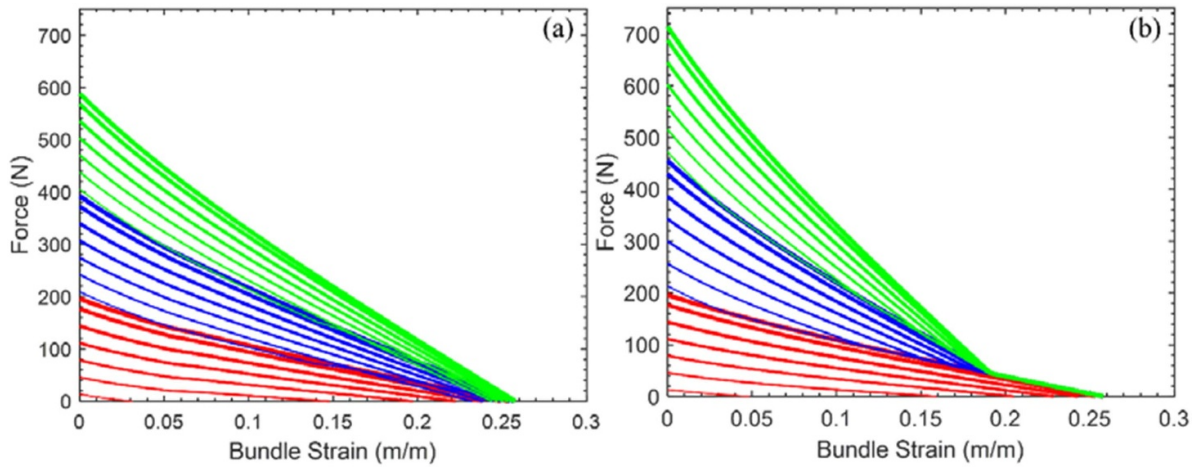

Figure 10. Analytical force–strain plots for the fixed-end (a) and tendoned (b) configurations for the EVC case at maximum strain. Varying line thickness is used to indicate pressure in each motor unit, and color is used to represent different recruitment states (red is RS1, blue is RS2, and green is RS3). All MUs in the fixed-end case still contain FAMs with a diameter of 6.35 mm, but the FAMs in MU2 and MU3 for the tendoned configuration have a larger diameter of 7.30 mm.

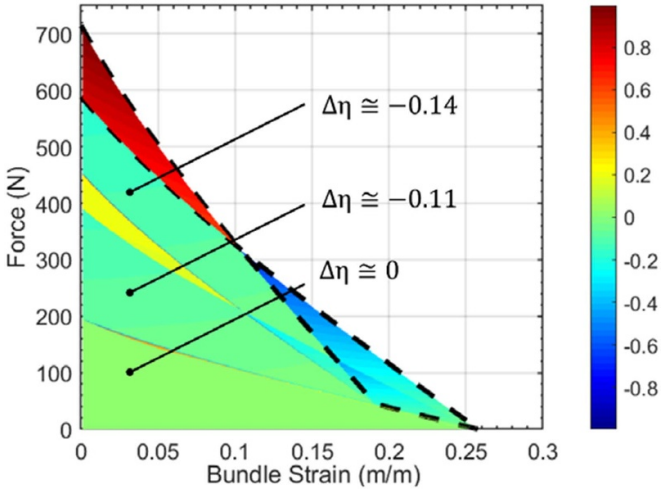

Figure 11. Surface plot of the efficiency difference between the tendoned and fixed-end configurations for the EVC case. The FAMs in each MU have the same parameters as the FAMs from the previous figure. The area enclosed by the dotted lines represents the part of the force–strain space that the two configurations do not have in common. The red dotted line area represents actuation that the tendoned configuration can provide, while the blue dotted line area represents actuation that the fixed-end configuration can provide.

RS2 over a larger range of strains than the fixed-end configuration.

This case study illustrates an important point: there is no case for which one configuration is uniformly superior to the other for the entire force–strain space with respect to isotonic efficiency. Instead, there are regions for which one performs better, and other regions for which one performs worse. Therefore, while we can use isotonic efficiency as an analysis tool, it does not definitively determine the superiority of one configuration over the other, and it is highly situational, depending on the application and region of operation.

4. Implications of fixed-end and tendoned configurations on bundle volumetric energy density

4.1. Actuator bundle spatial envelope

In addition to the traditional efficiency metrics that can be used to evaluate the tendoned and fixed-end configurations, we can also evaluate the spatial envelope of the two configurations at different recruitment states. In the fixed-end configuration, inactive and low-pressure FAMs will buckle outward and even collapse at certain values of strain. In a real-world application, this might be undesirable for several reasons. For one, FAMs that buckle outward may violate tight spatial constraints or tolerances that might be necessary for a given application. Additionally, the outward buckling of FAMs in a bundle may limit the number of actuators that can be placed within a given space, which would affect the maximum actuation potential of a bundle. Consider the three-MU bundle presented in figure 12, where each MU consists of a single FAM and the FAMs are arranged in a triangular cross section. It is important to note that this bundle falls under the ER case, where all three FAM have the same radii. In recruitment state 1, MU1 is active and contracting and MU2 and MU3 are inactive. These inactive MUs will generate resistive forces and buckle outward, and if compressed far enough, they will collapse and their mode shapes will change, as shown previously in figure 1. When MU2 and MU3 buckle outward, this increases the total spatial envelope occupied by the bundle. If we discretize each FAM along its length, we can approximate the overall volume envelope of the bundle by making a few simplifying assumptions. First, we assume that at a given pressure and strain, the cross-sectional area of each FAM remains both circular and constant along its length. We also assume that if a FAM is in the pre-buckled region (i.e. before free strain), it experiences no transverse deflection and that if a FAM buckles, it buckles outward in the radial direction. Because we assume outward buckling, the calculated volume envelope will be the maximum possible

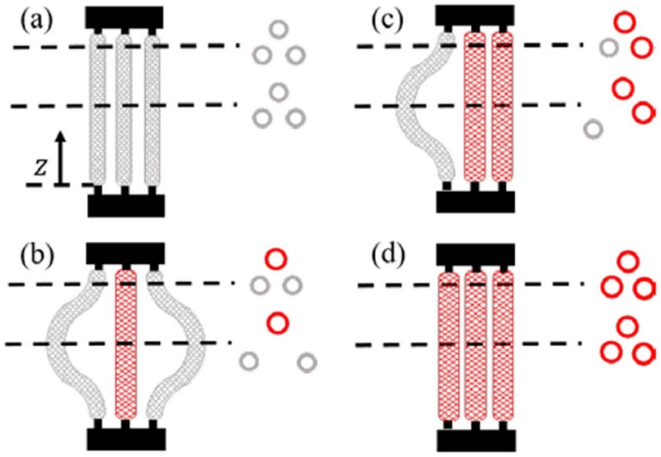

Figure 12. Illustration of the cross-sectional area profiles at different z-locations for an inactive bundle (a), a bundle in RS1 (b), RS2 (c) and RS3 (d). For RS1 and RS2, the outward buckling of the inactive FAMs significantly changes the distance and spacing between the FAM cross sections. If the bundle is discretized lengthwise with a suitable resolution, these different area cross-sections can be added up to calculate the spatial envelope volume.

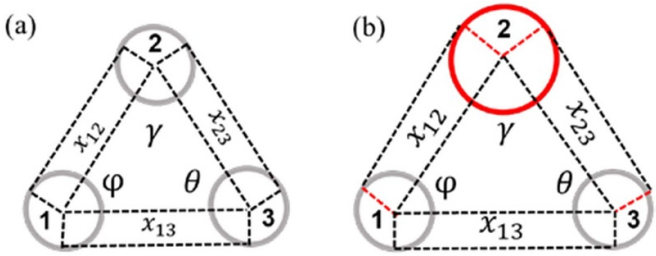

Figure 13. Envelope cross sections used for calculating FAM volumetric envelope for the situation in which all three MUs are inactive (a) and in which MU1 is actively pressurized and contracting while MU2 and MU3 are inactive (b), eventually buckling outward and collapsing. Instead of rectangles used to calculate the area, trapezoids must be used.

volume envelope for a given bundle configuration. Finally, we assume that the initial spacing between the centerline of each FAMs is equal to the sum of the radii of the two FAMs at free contraction with maximum operating pressure. Figure 12 illustrates how the cross-sectional profile changes for different positions z along the length of the bundle at different recruitment states.

Now let us consider two different situations: in the first situation, all three FAMs are at the same pressure, implying that they are all inactive or fully pressurized, and in the second situation, MU1 is pressurized and MU2 and MU3 are inactive. A more detailed depiction of the envelope cross-sectional areas for these two situations is shown in figure 13.

When all three MUs are at the same pressure, the cross-sectional area can be approximated using an equilateral triangle, three rectangles, and three circular sectors. When all three MUs are at different pressures, as strain is increased, since MU1 is pressurized, its radius increases, and since MU2 and MU3 are inactive, their radii stay the same, resulting in a trapezoid between MU1 and MU2/MU3 instead of a rectangle. To approximate the area of this trapezoid, it is assumed that the parallel sides of each trapezoid (shown in red in figure 13) are equal to the radius of the circle in which it resides and that the outer non-parallel side of each trapezoid is tangent to a point collinear with the parallel side. This assumption would only cause a significant difference if the cross-sectional area of one FAM is significantly larger than the cross-sectional area of the other FAM. Since this is not the case, the area of the trapezoidal portions can be approximated as:

$$A_{\text{trap}} = \frac{1}{2}\left[x_{12}\left(R_1+R_2\right)+x_{23}\left(R_2+R_3\right)+x_{13}\left(R_1+R_3\right)\right] \tag{11}$$

where R_1, R_2 and R_3 are the instantaneous outer radii of MU1, MU2, and MU3, respectively.

The area of the triangle connecting the midpoints of all three FAMs is given by:

$$A_{\text{tri}} = \sqrt{s\left(s-x_{12}\right)\left(s-x_{23}\right)\left(s-x_{13}\right)} \tag{12}$$

where s is the semiperimeter of the triangle (the sum of the side lengths divided by two).

The combined area of the circular sectors is calculated as follows:

$$A_{\text{circ}} = \pi(R_1)^2\left(\frac{\pi-\varphi}{2\pi}\right)+\pi(R_2)^2\left(\frac{\pi-\gamma}{2\pi}\right) + \pi(R_3)^2\left(\frac{\pi-\theta}{2\pi}\right). \tag{13}$$

For the two situations shown in figure 13, the angles are known since the triangle remains equilateral. However, when all three MUs are at different pressures, the outward deflections of each MU will be different, and as a result, this triangle will no longer be equilateral, meaning the angle values will need to be calculated (which is why they have been included in this formulation).

To calculate these areas for a given cross section, we need to know the outer radii of each motor unit for a given pressure and strain. These radii can be determined for the Nth motor unit using a typical FAM contraction function, which can be found in [1]

$$R_N\left(\varepsilon_N\right) = R_{0,N} f\left(\varepsilon_N\right). \tag{14}$$

We also need to know the initial centerline distance between motor units, defined for MU1 and MU2 as the sum of the maximum radii of each MU:

$$x_{0,12} = R_{0,1} f\left(\varepsilon_{1,\text{free}}\right) + R_{0,2} f\left(\varepsilon_{2,\text{free}}\right). \tag{15}$$

A similar calculation can be made for the other centerline distances. The centerline distance as a function of ε and z can be calculated as:

$$x_{12} = x_{0,12} + y_1\left(z,\varepsilon_1\right) + y_2\left(z,\varepsilon_2\right) \tag{16}$$

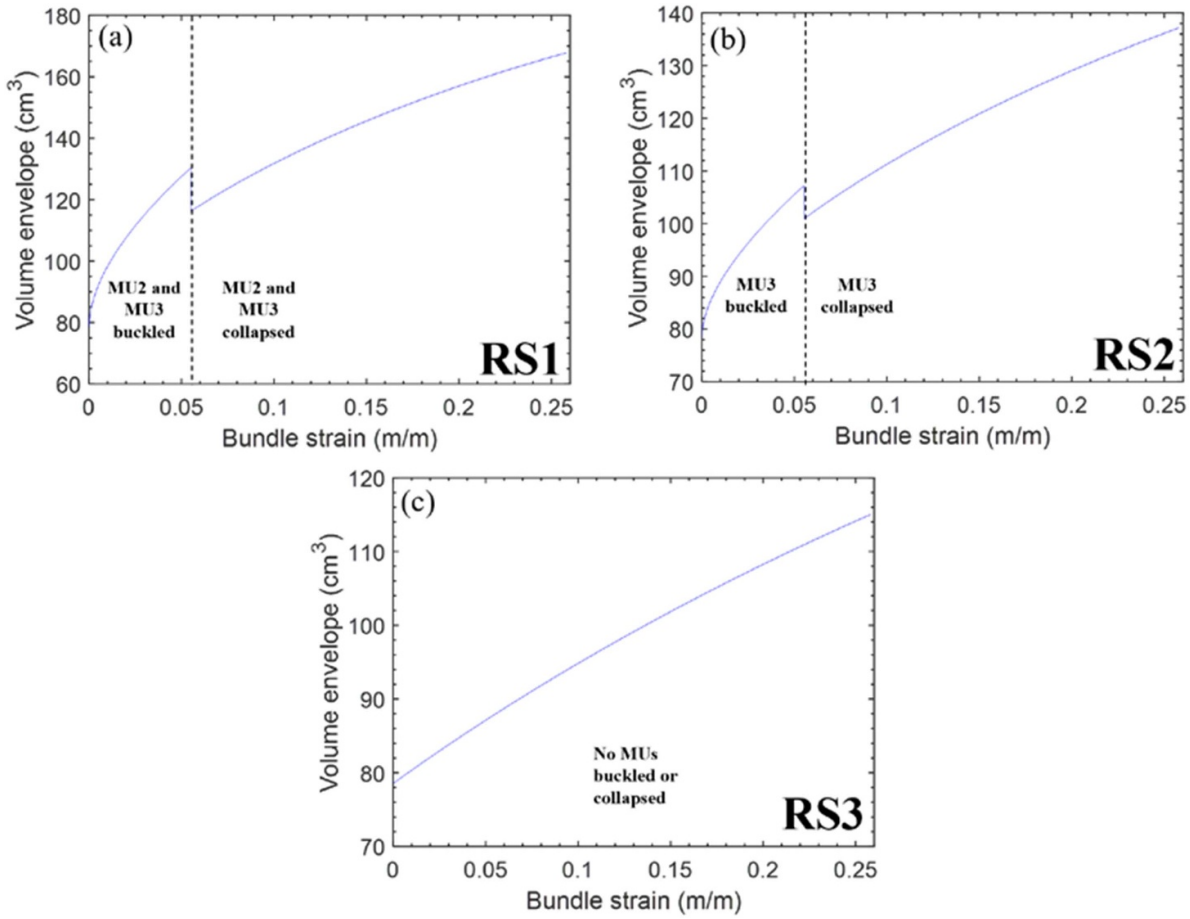

Figure 14. Plot of fixed-end bundle volume envelope vs. bundle strain for (a) RS1 at full activation, (b) RS2 at full activation, and (c) RS3 at full activation. FAM parameters are the same as they were in the ER case portrayed in figure 6. Each MU contains a single FAM with an initial outer radius of 6.35 mm, an initial inner radius of 4.76 mm, an initial braid angle of 33 degrees, and an overall bundle length of 127 mm. The dashed lines demonstrate the boundary between the post-buckling and post-collapse regions of the inactive FAMs in the bundle.

where y_1 and y_2 are the transverse deflections of MU1 and MU2, respectively. The value of the transverse deflection of a FAM is dependent on whether the FAM is in a contracted, buckled, or collapsed state. If a FAM is in a contracted state, it has not exceeded free strain and experiences zero transverse deflection. A FAM in a buckled state has exceeded free strain and begins to deflect outward. The mode shape for this outward deflection, as a function of lengthwise FAM location, is assumed to follow:

$$y(z) = \frac{y_{\max}(\varepsilon_N)}{2}\left[\cos\left(\frac{2\pi}{L_{\text{bun}}}z\right)+1\right] \tag{17}$$

where L_{bun} is the entire length of the bundle. If a FAM is in the collapsed state, it has already been in the buckled state and its transverse deflection shape is assumed to be:

$$y(z) = \frac{y_{\max}(\varepsilon_N)}{2}\left[1-\cos\left(\frac{2\pi}{L_{\text{bun}}}z\right)\right]. \tag{18}$$

The point at which the FAM transitions between the buckled state and the collapsed state, as well as the maximum transverse deflection $y_{\max}$ (which is a function of strain), are given in the model developed by Kim *et al* [22]. Now that we have everything necessary to calculate centerline distance as a function of lengthwise location and strain, we can calculate the area of every lengthwise cross-sectional profile and numerically integrate along the length of the system to find the volume envelope of the entire bundle as a function of pressure and strain:

$$V_{\text{env}} = \int_0^{L_{\text{bun}}} (A_{\text{trap}} + A_{\text{tri}} + A_{\text{circ}})\, dz. \tag{19}$$

Using these equations, we can find the volume envelope for different operating points within the bundle force–strain space. For example, figure 14 illustrates the volumetric envelope as a function of strain for maximal activation of RS1, RS2, and RS3 when all three MUs have the same radius. The plot has been annotated to illustrate the states of each MU (contracted, buckled, collapsed) and where they occur for each recruitment state and strain.

Figure 16 plots the resulting volumetric envelope as a function of strain for maximal activation of all three recruitment states for the tendoned configuration for the ER case. From

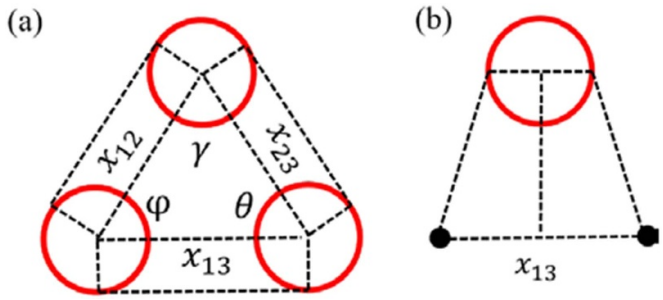

Figure 15. The cross section shown in (a) represents the area slice at z-locations within the length of the MU2 and MU3 FAMs, while the cross section shown in (b) represents the area slice at z-locations beyond the ends of the MU2 and MU3 FAMs. The presence of the tendons is denoted by the solid black circles. The tendons themselves are assumed to be of sufficiently small diameter such that their cross sections contribute negligible area to the total envelope cross sectional area.

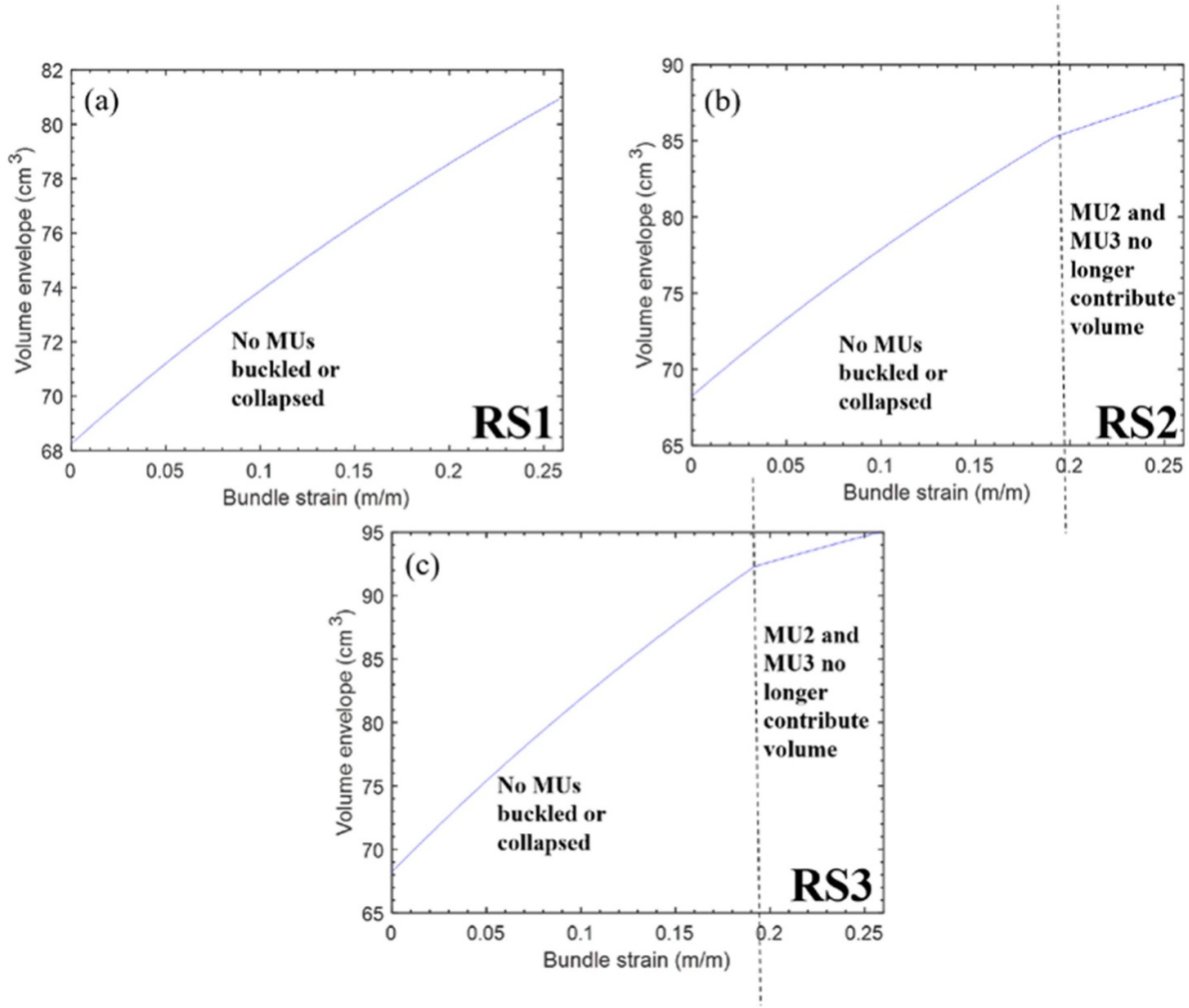

Figure 16. Plot of tendoned bundle volume envelope vs. bundle strain for (a) RS1 at full activation, (b) RS2 at full activation, and (c) RS3 at full activation. Each MU contains a single FAM with an initial outer radius of 6.35 mm, an initial inner radius of 4.76 mm, an initial braid angle of 33 degrees, and an overall bundle length of 127 mm. FAM parameters are the same as they were in the ER case portrayed in figure 6. The dashed lines demonstrate the boundary between the post-buckling and post-collapse regions of the inactive FAMs in the bundle.

these plots, it can be seen that the volume envelope for RS1 and RS2 is greater than that for RS3 due to the outward deflection of inactive motor units. Within RS1 and RS2, the slope of the volume envelope curves changes at the collapse point of the inactive FAMs, since the mode shape (and therefore, the transverse deflection) of these FAMs changes. The volumetric envelope can be calculated in a similar manner for the tendoned configuration. If the tendon is properly sized (as shown in section 2), then there will be no outward buckling or resistive forces at any operating point within the bundle force–strain

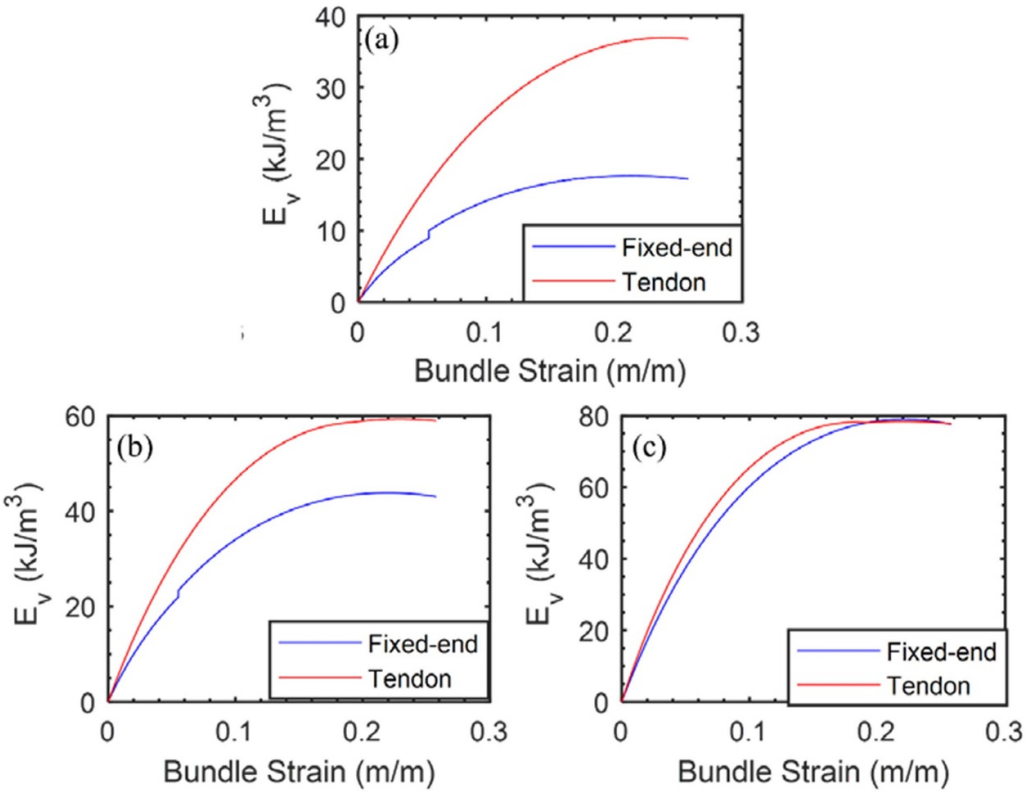

Figure 17. Plot of fixed-end and tendoned bundle volumetric energy density vs. bundle strain for (a) RS1 at full activation, (b) RS2 at full activation, and (c) RS3 at full activation. Each MU contains a single FAM with an initial outer radius of 6.35 mm, an initial inner radius of 4.76 mm, an initial braid angle of 33 degrees, and an overall bundle length of 127 mm. The tendoned FAMs have a length of 94.2 mm, while the tendoned bundle is the same overall length as the fixed-end bundle (127 mm).

space. As a result, there will be no transverse deflection in the tendoned FAM bundle, and the cross-sectional profile of the bundle will remain the same at all lengthwise locations within the FAMs. In addition, the tendoned FAMs will be shorter than the fixed-end FAMs. To adjust for this difference in length, at all lengthwise locations beyond the end of the tendoned FAMs, a trapezoidal cross-section connecting the tendon locations and the diameter of MU1, along with a semicircular area for the rest of MU1, is used. This is illustrated in the figure 15:

For most of the strain range in these plots, the volume envelope for the tendoned configuration for each recruitment state looks similar to the RS3 volume envelope for the fixed-end configuration. However, for RS2 and RS3, at the local free strain of the FAMs in MU2 and MU3, there is a distinct slope change, and the volumetric envelope begins to increase at a slower rate. This is because past this strain value, the two tendoned FAMs cease increasing in diameter because of their shorter overall length and therefore do not contribute to any further increases in volumetric envelope.

4.2. Volumetric energy density comparison

While the volume envelope of a configuration for a given strain and recruitment state determines how much space a bundle occupies, we can use volumetric energy density to quantify how bundle envelope changes affect performance throughout the force–strain space. To calculate the volumetric energy density associated with maximal activation of a given RS, we first calculate the work output when contracting the bundle to a given strain with constant source pressure applied to all active motor units. This isobaric work is given as:

$$W_{\text{isobaric}} = \int_0^{\varepsilon_{\text{bun}} L_{\text{bun}}} F_{\text{bun}}(P, \varepsilon_{\text{bun}})\, dz \tag{20}$$

where $F_{\text{bun}}(P, \varepsilon_{\text{bun}})$ is the bundle force for a given pressure and system strain and dz is a differential lengthwise element. Volumetric energy density is then given by:

$$E_{\text{v}} = \frac{W_{\text{isobaric}}(P, \varepsilon_{\text{bun}})}{V_{\text{env}}(P, \varepsilon_{\text{bun}})} \tag{21}$$

where $V_{\text{env}}(P, \varepsilon_{\text{bun}})$ is the maximum volume envelope as a function of pressure and system strain, as calculated in equation (19). We can generate plots for a bundle in each configuration that allows for the comparison of volumetric energy density for the ER case at different points throughout the force–strain space.

Figure 17 shows that at full activation of each recruitment state (with the exception of recruitment state 3 at very high strain values), the tendoned configuration offers superior energy density to the fixed-end configuration. For RS1, at maximum strain and maximal activation, the volumetric energy density for the tendoned configuration is more than three times

that that of the fixed-end configuration. At the full activation of RS2, MU2 is no longer buckled outward, which explains why the gap in volumetric energy density between the two configurations is reduced. At the full activation of RS3, neither MU2 nor MU3 is buckled outward, reducing the gap even more. However, even at the full activation of RS3, the tendoned configuration remains favorable to the fixed-end until the tendoned FAMs reach their own local free strain, at which point the fixed-end configuration becomes marginally more favorable.

The significance of these results is that despite the fact that, for a bundle of FAMs with the same radius, the tendoned configuration provides a smaller overall force–strain space than the fixed-end configuration due to less maximum contraction in MU2 and MU3, it makes up for this by being more energy dense than the fixed-end configuration in all three recruitment states. This is because in the tendoned configuration, inactive FAMs do not buckle outward, resulting in a smaller overall spatial envelope. As a result, for an equivalent volume envelope, the space saved by the tendoned configuration would allow for more potential actuation, or inclusion of other system components within the space, both of which are extremely valuable in the design of robotic systems.

5. Conclusion

In this paper, we have introduced a tendon-based resistive force mitigation strategy and presented analysis tools with which this strategy can be evaluated. By attaching inextensible tendons to certain motor units in a variable recruitment bundle and sizing these tendons appropriately, resistive force generation and outward buckling of these motor units can be eliminated. The benefit of this resistive force elimination is that it can increase efficiency in some regions of the force–strain space, and the benefit of the elimination of outward buckling is that it reduces the overall spatial envelope of the bundle, thereby increasing its volumetric energy density. The performance of a three-MU variable recruitment bundle was compared for both a traditional fixed-end configuration and the novel tendoned configuration presented in this paper by imposing the constraint that the overall bundle length for both configurations must be the same. Due to this constraint, the overall tendoned FAM lengths in MU2 and MU3 were reduced, making these MUs unable to contribute force over the full system contraction range. This resulted in less overall actuation potential in the tendoned configuration for the case of equal FAM radii (ER case) in each MU. However, when the tendoned FAMs were sized for equal volume consumption at maximum system strain (EVC case), the tendoned configuration had higher blocked force and made up for the decreased actuation potential at higher strain values by allowing for increased actuation potential at higher force values. Isotonic efficiency was compared for the shared force–strain space for both the ER case and EVC case. For the ER case, the tendoned configuration was slightly more efficient for a large part of the force–strain space, but experienced reduced efficiency at the boundary between RS2 and RS3 due to the reduced local free strain in the upper motor units. Inversely, for the EVC case, the fixed-end configuration was marginally more efficient for a large part of the force–strain space, but experienced reduced efficiency between recruitment states 2 and 3 since the MUs with tendons had higher blocked force values. Overall, the isotonic efficiency values for the fixed-end and tendoned configurations are very comparable regardless of the case being studied, with advantages and disadvantages appearing in different parts of the force–strain space. As a result, if isotonic efficiency is the sole evaluation metric, the decision of whether to use the fixed-end or the tendoned configuration is highly situational. We also considered a second metric to evaluate each configuration's spatial envelope: volumetric energy density. Since the FAMs in the traditional fixed-end configuration buckle outward, the maximum volume envelope of this configuration is much larger than that of the tendoned configuration. As a result, the volumetric energy density of the fixed-end configuration is much smaller for nearly the entire shared force–strain space. At maximal activation of RS1, the minimum volumetric energy density of the tendoned configuration is more than three times that of the fixed-end configuration. This demonstrates that by using the tendoned configuration, up to three times the amount of actuation can be achieved. With comparable isotonic efficiency metrics and superior spatial efficiency, the tendoned configuration offers an attractive and readily-implemented solution to the problem of resistive forces and outward buckling of traditional fixed-end variable recruitment bundles.

Data availability statement

All data that support the findings of this study are included within the article.

All data that support the findings of this study are included within the article (and any supplementary files).

Funding

This work was supported primarily by the Faculty Early Career Development Program (CAREER) of the National Science Foundation under NSF Award No. 1845203 and Program Manager Irina Dolinskaya. Additionally, this material is based upon work supported by the National Science Foundation Graduate Research Fellowship Program under Grant No. 1650114. Any opinions, findings and conclusions or recommendations expressed in this material are those of the author(s) and do not necessarily reflect those of the National Science Foundation.

Author contributions

Conceptualization, N M, J Y K and M B; Funding acquisition, M B; Investigation, N M and J Y K; Methodology, N M and J Y K; Resources, M B; Supervision, M B; Validation, N M; Visualization, N M and J Y K; Writing—original draft, N M and J Y K; Writing—review and editing, M B. All authors have read and agreed to the published version of the manuscript.

Conflict of interest

The authors declare no conflicts of interest.

ORCID iDs

Nicholas Mazzoleni https://orcid.org/0000-0002-9377-849X
Jeong Yong Kim https://orcid.org/0000-0001-9895-9807

References

[1] Tondu B 2012 Modelling of the McKibben artificial muscle: a review *J. Intell. Mater. Syst. Struct.* **23** 225–53
[2] Garbulinski J, Balasankula S C and Wereley N M 2021 Characterization and analysis of extensile fluidic artificial muscles *Actuators* **10** 26
[3] Tondu B and Lopez P 1997 The McKibben muscle and its use in actuating robot-arms showing similarities with human arm behaviour *Ind. Robot Int. J.* **24** 432–9
[4] Kang B-S, Kothera C S, Woods B K and Wereley N M 2009 Dynamic modeling of Mckibben pneumatic artificial muscles for antagonistic actuation *2009 IEEE Int. Conf. on Robotics and Automation* (IEEE) pp 182–7
[5] Henneman E, Somjen G and Carpenter D O 1965 Excitability and inhibitibility of motoneurons of different sizes *J. Neurophysiol.* **28** 599–620
[6] Bryant M, Meller M A and Garcia E 2014 Variable recruitment fluidic artificial muscles: modeling and experiments *Smart Mater. Struct.* **23** 074009
[7] Meller M, Chipka J, Volkov A, Bryant M and Garcia E 2016 Improving actuation efficiency through variable recruitment hydraulic McKibben muscles: modeling, orderly recruitment control, and experiments *Bioinsp. Biomim.* **11** 065004
[8] DeLaHunt S A, Pillsbury T E and Wereley N M 2016 Variable recruitment in bundles of miniature pneumatic artificial muscles *Bioinsp. Biomim.* **11** 056014
[9] Jenkins T E, Chapman E M and Bryant M 2016 Bio-inspired online variable recruitment control of fluidic artificial muscles *Smart Mater. Struct.* **25** 125016
[10] Chapman E M, Jenkins T and Bryant M 2018 Design and analysis of electrohydraulic pressure systems for variable recruitment in fluidic artificial muscles *Smart Mater. Struct.* **27** 105024
[11] Chipka J, Meller M A, Volkov A, Bryant M and Garcia E 2017 Linear dynamometer testing of hydraulic artificial muscles with variable recruitment *J. Intell. Mater. Syst. Struct.* **28** 2051–63
[12] Loccisano A 2020 Online variable recruitment for pneumatic artificial muscles with springs *Master's Thesis* KTH Royal Institute of Technology, School of Industrial Engineering and Management
[13] Robinson R M, Kothera C S and Wereley N M 2014 Variable recruitment testing of pneumatic artificial muscles for robotic manipulators *IEEE/ASME Trans. Mech.* **20** 1642–52
[14] Kim J Y, Mazzoleni N and Bryant M 2021 Investigation of resistive forces in variable recruitment fluidic artificial muscle bundles *Top. Mod. Anal. Test.* **8** 305–13
[15] Kim J Y, Mazzoleni N and Bryant M 2021 Modeling of resistive forces and buckling behavior in variable recruitment fluidic artificial muscle bundles *Actuators* **10** 42
[16] Klute G K and Hannaford B 2000 Accounting for elastic energy storage in McKibben artificial muscle actuators *J. Dyn. Syst. Meas. Control* **122** 386–8
[17] Yu Z, Pillsbury T, Wang G and Wereley N M 2019 Hyperelastic analysis of pneumatic artificial muscle with filament-wound sleeve and coated outer layer *Smart Mater. Struct.* **28** 105019
[18] Kothera C S, Jangid M, Sirohi J and Wereley N M 2009 Experimental characterization and static modeling of McKibben actuators *J. Mech. Des.* **131** 091010
[19] Ball E and Garcia E 2016 Effects of bladder geometry in pneumatic artificial muscles *J. Med. Dev.* **10** 041001
[20] Meller M A, Bryant M and Garcia E 2014 Reconsidering the McKibben muscle: energetics, operating fluid, and bladder material *J. Intell. Mater. Syst. Struct.* **25** 2276–93
[21] Tondu B and Lopez P 2000 Modeling and control of McKibben artificial muscle robot actuators *IEEE Control Syst. Mag.* **20** 15–38
[22] Colbrunn R W, Nelson G M and Quinn R D 2001 Modeling of braided pneumatic actuators for robotic control *Proc. 2001 IEEE/RSJ Int. Conf. on Intelligent Robots and Systems. Expanding the Societal Role of Robotics in the The Next Millennium (Cat. No. 01CH37180)* vol 4 (IEEE) pp 1964–70